JOURNAL OF THEORETICAL
AND APPLIED MECHANICS
3, **37**, 1999

NUMERICAL EVALUATION OF SENSITIVITY OF STRESS DISTRIBUTION IN BONE TO GEOMETRIC PARAMETERS OF ENDOPROSTHESIS

PIOTR KOWALCZYK

Institute of Fundamental Technological Research, Polish Academy of Sciences
e-mail: pkowalcz@ippt.pan.pl

One of serious drawbacks in the bone endoprosthetics is the implant separation from bone or cement. Stress concentrations on the implant surface are deemed major factor in this process and implant shape optimization seems to be a natural way of improvement of stress distribution. An important tool in effective optimization algorithms is the design sensitivity analysis (DSA).
The discretized formulation of the problem in terms of the finite element method is presented in this paper. A three-dimensional model of femur with a cementless implant is analysed. Frictionless contact and perfect bonding are assumed on the smooth and rough parts of the implant surface, respectively. Computational examples show the stress concentrations and their sensitivity to various geometric parameters of the implant.

Key words: biomechanics, sensitivity analysis, finite element method, contact problems

1. Introduction

Bone implantation (endoprosthetics) is a standard surgical technique employed in treatment of joint failures, especially in hips and knees. It consists in replacement of the disfunctional joint with an artificial one. The latter may be connected with the skeletal bones in various ways. The most common one consists in drilling a hole in the living bone and either enforced pressing the implant into the bone (cementless endoprosthesis) or filling the hole with polymeric cement and placing the implant in it (cemented endoprosthesis).

One of serious drawbacks of this technique consist in separation of the implant from either bone tissue or cement occurring after certain period of time. The main reason is bone fracture or degradation around the implant surface. Also, in the case of cemented implants, mechanical failure of the aging cement plays a role in the failure of the entire bone-cement-implant system.

In either case, unnatural stress distribution is considered to be the main reason for the failure. The implant is much stiffer than the bone tissue which results in some areas of bone being understressed (stress-shielded) and some other – subject to extreme stress concentration. Little is known so far about precise failure criteria. Kuiper and Huiskes (1997) suggested that surface shear stress might play a major role in crack development in bone tissue. Hedia et al. (1996) introduced the notion of *fatigue notch factor* being a functional of the equivalent stress distribution. This factor is deemed responsible for mechanical damage of a cement layer around cemented implant, but may also affect the damage of bone tissue around the cementless implant. The strain energy is believed to affect the bone degradation in understressed areas (Kuiper and Huiskes, 1997).

It is widely believed that optimization of the implant properties may significantly improve the reliability of joint endoprostheses. Thus, among numerous papers devoted to equilibrium analysis of the bone-implant systems (Kang et al., 1993; Keaveny and Bartel, 1993; Mann et al., 1995; McNamara et al., 1997; Dammak et al., 1997; and many others) appearing in the literature, the issue of design optimization has been raised (Yang et al., 1984) and has become of increasing interest in the recent years (Hedia et al., 1996, 1997; Kuiper and Huiskes, 1997). The design parameters are either material constants of the implant (which is the simplest case from the computational point of view but has little practical implications) or shape parameters. Optimization of the latter seems most promising in terms of the expected improvement. So far, only two-dimensional linearly elastic models have been discussed, which poses essential limitations on the results precision and reliability.

The design sensitivity analysis (DSA) is a crucial tool in most advanced and efficient optimization algorithms. Theoretical background for numerical applications was presented by Haug et al., 1986; nonlinear finite-element aspects were discussed extensively by Kleiber et al. (1997). Many finite element codes provide now the feature of DSA in the linear range as an add-on to the equilibrium analysis. However, both the equilibrium and sensitivity results obtained for nonlinear material and/or geometric behavior of the structure may significantly differ from the linear approximations. In the bone-implant analysis this may occur when contact boundary conditions on the implant interface are to be considered.

The present paper provides a three-dimensional numerical model of a bone-implant system offering the possibility of sensitivity analysis. The femur with a cementless endoprosthesis is chosen as an example. Since the main goal is to test the numerical algorithm and the developed software rather than to obtain precise results, some simplifying assumptions about the material and geometric model are made. The bone model is symmetric with respect to the longitudinal plane and all cross-sections are piecewise semi-elliptic. Two types of boundary conditions are assumed on the bone-implant interface: perfect bonding on the rough (porous-coated) part of the implant surface (tissue ingrowth into the surface pores is thus allowed) and frictionless sliding on the smooth part of the implant surface. The bone material is assumed isotropically elastic with different material constants for cortical and spongeous bone tissues. The stress distribution on the bone-implant interface is analysed. The analysis is followed by the sensitivity analysis with geometric parameters defining the implant shape taken as design variables.

2. Formulation of the problem

2.1. Continuum eqautions

The displacement formulation of a geometrically linear solid equilibrium problem in the Cartesian coordinate system has the following form

$$\sigma_{ij,j} - f_i = 0 \qquad \text{in } \Omega \tag{2.1}$$

where

σ_{ij} – stress
f_i – mass forces
Ω – area occupied by material.

The indices i, j run over the values 1,2,3. Stress is related to the unknown displacement field u_i via the constitutive equation

$$\sigma_{ij} = \sigma_{ij}(\varepsilon_{kl}) \tag{2.2}$$

and the geometric equation

$$\varepsilon_{ij} = \frac{1}{2}(u_{i,j} + u_{j,i}) \tag{2.3}$$

where ε_{ij} stands for strain and $\sigma_{ij}(\varepsilon_{kl})$ is a known function. For elastic materials

$$\sigma_{ij}(\varepsilon_{kl}) = C_{ijkl}\varepsilon_{kl} \tag{2.4}$$

The constitutive equations employed in the particular problem of bone-implant analysis will be discussed in Section 2.4.

The boundary conditions on the external surface of Ω are as follows

$$\begin{aligned} \sigma_{ij} n_j &= \hat{t}_i \qquad \text{on} \quad \partial\Omega^\sigma \\ u_i &= \hat{u}_i \qquad \text{on} \quad \partial\Omega^u \end{aligned} \tag{2.5}$$

where $\hat{t}_i$ and $\hat{u}_i$ are known.

Contact surfaces within Ω are handled as follows. If this is a perfect-bonding surface, it is treated as an internal surface where Eq (2.1) holds. If this is a slide surface, Eq $(2.5)_1$ holds on both sides (i.e. for each contacting body separately) with the same value of $\hat{t}_i = t_i^{(c)}$ which is, however, unknown

$$\sigma_{ij} n_j = t_i^{(c)} \qquad \text{on} \quad \partial\Omega^c \tag{2.6}$$

If the frictionless contact is considered, then a normal (i.e. parallel to n_i) component of $t_i^{(c)}$ is the only non-zero one. For numerical reasons, we will slightly weaken the latter contact condition by allowing for a non-zero penetration d on the contact surface, and relating the normal contact force $t_n^{(c)}$ to d with the equation

$$t_n^{(c)} = -kd \tag{2.7}$$

where k is an arbitrary penalty coefficient determined on the basis of stiffness coefficients and dimensions of the contacting bodies. For negative d (contact clearance), k is assumed zero.

2.2. Finite element formulation

In the finite element method (Zienkiewicz, 1977) an approximate solution is sought in the class of linear combination of the shape functions $\Psi_{i\alpha}$

$$u_i(x_k) = \Psi_{i\alpha}(x_k) q_\alpha \qquad \alpha = 1, \ldots, N \tag{2.8}$$

where q_α are unknown parameters which in physical sense, at a certain choice of the shape function form, represent values of the displacement components at selected material points called nodes. The functions are defined on subdomains of Ω called elements and are continuous in Ω and differentiable within each element.

Substitution of Eq (2.8) into Eqs (2.1)-(2.5) and application of the Galerkin method leads to the following equation

$$F_\alpha = Q_\alpha \tag{2.9}$$

where

$$F_\alpha = \int_\Omega B_{k\alpha}\sigma_k \, d\Omega \tag{2.10}$$

is the internal nodal force vector

$$Q_\alpha = \int_\Omega \Psi_{i\alpha} f_i \, d\Omega + \int_{\partial\Omega^\sigma} \Psi_{i\alpha}\hat{t}_i \, d(\partial\Omega) \tag{2.11}$$

is the external nodal load

$$B_{k\alpha} = \frac{d\varepsilon_k}{dq_\alpha} \tag{2.12}$$

is the geometric matrix consisting of properly ordered spatial derivatives of $\Psi_{i\alpha}$, and σ_k, ε_k, $k = 1, \ldots, 6$, denote the stress and strain component vectors, respectively, expressed in the so-called finite-element vector/matrix notation:

$$\begin{aligned} \{\sigma_k\} &:= \{\sigma_{11}, \sigma_{22}, \sigma_{33}, \sigma_{23}, \sigma_{31}, \sigma_{12}\} \\ \{\varepsilon_k\} &:= \{\varepsilon_{11}, \varepsilon_{22}, \varepsilon_{33}, 2\varepsilon_{23}, 2\varepsilon_{31}, 2\varepsilon_{12}\} \end{aligned}$$

(symmetry of both the stress and strain tensors is assumed). The elastic constitutive tensor components C_{ijkl} are written in this notation as a 6×6 matrix C_{mn}.

The shape functions $\Psi_{i\alpha}$ are defined according to the linear isoparametric element concept (Zienkiewicz, 1977). Cubic (8-node), prismatic (6-node), pyramidal (5-node) and tetrahedral (4-node) elements are used in the numerical examples below.

The contact equations (2.6) and (2.7) are modelled as follows. A fictitious zone Ω^c between the contacting surfaces is introduced. It is filled with a medium whose constitutive equation is

$$\begin{aligned} \sigma_k &= t_n^{(c)}\{1, 1, 1, 0, 0, 0\} \\ t_n^{(c)} &= \begin{cases} k\bar{J}\dfrac{\bar{A}\bar{d}}{A_0} = k'\bar{J} & \text{for} \quad \bar{J} \geqslant 0 \\ 0 & \text{for} \quad \bar{J} < 0 \end{cases} \end{aligned} \tag{2.13}$$

where k is the coefficient from Eq (2.7), A_0 is the initial area of potential contact zone and $\bar{J}$ is the volumetric deformation of the contact zone with respect to a reference configuration $\overline{C}^c$ in which the zone area $\bar{A}$ and thickness $\bar{d}$ are finite and constant. In other words

$$\bar{J} = \det[\bar{F}_{ij}]$$

where $\bar{F}_{ij}$ is the deformation gradient from $\overline{\Omega}^c$ to Ω^c. This is a numerical approximation of Eq (2.7) that penalizes possible penetration of the contacting bodies. Note that $\bar{J}$ can take zero or negative values.

Detailed presentation and discussion of this finite element contact model can be found in Kowalczyk (1994). Let us only recall that the contact forces contribution to the internal nodal force equals

$$F_\alpha^c = \int_{\overline{\Omega}^c} k' \Psi_{i\alpha;j} \bar{J}^2 \bar{F}_{ji}^{-1} \, d\Omega^c \tag{2.14}$$

where $(\cdot)_{;i}$ denotes differentiation with respect to spatial coordinates in $\overline{C}^c$. This contribution should be added to the vector F_α computed from Eq (2.10). Eq (2.9) with contact phenomena included should thus read

$$F_\alpha + F_\alpha^c = Q_\alpha \tag{2.15}$$

Eq (2.15) is thus generally a nonlinear (however, in the small-strain elastic case, linear) equation with respect to unknown vector q_α, $\alpha = 1, \ldots, N$. To solve it, the Newton-Raphson scheme is employed in which subsequent corrections to the current approximate solution are found from the equation

$$K_{\alpha\beta} \delta q_\beta = Q_\alpha - (F_\alpha + F_\alpha^c) \tag{2.16}$$

with

$$K_{\alpha\beta} = \frac{d(F_\alpha + F_\alpha^c - Q_\alpha)}{dq_\beta} \tag{2.17}$$

being the tangent stiffness matrix of the structure. Neglecting the dependence of Q_α on q_α we can write

$$\begin{aligned} K_{\alpha\beta} = & \int_\Omega B_{m\alpha} C_{mn} B_{n\beta} \, d\Omega + \\ & + \int_{\overline{\Omega}^c} k' \Psi_{i\alpha;j} \Big(2 \bar{F}_{lk}^{-1} \bar{F}_{ji}^{-1} - \bar{F}_{li}^{-1} \bar{F}_{jk}^{-1} \Big) \Psi_{k\beta;l} \bar{J}^2 \, d\Omega^c \end{aligned} \tag{2.18}$$

In the small-strain elastic case Eq (2.15) becomes linear and the solution is found from

$$K_{\alpha\beta} q_\beta = Q_\alpha \tag{2.19}$$

Having the solution q_α we are able to compute any structural response $\phi(q_\alpha)$ (stress, strain, energy, etc.).

2.3. Design sesitivity analysis

The goal of the design sesitivity analysis (DSA) is to compute the total derivative of structural response $\phi(q_\alpha, h)$ with respect to design parameter h. Let us write it in the form

$$\frac{d\phi}{dh} = \frac{d\phi}{dh}\Big|_{q_\alpha \neq q_\alpha(h)} + \frac{d\phi}{dq_\alpha}\frac{dq_\alpha}{dh} \tag{2.20}$$

We have to find the unknown dq_α/dh from the following equation (cf Eq (2.15))

$$K_{\alpha\beta}\frac{dq_\beta}{dh} = \frac{d(Q_\alpha - F_\alpha)}{dh}\Big|_{q_\alpha \neq q_\alpha(h)} \tag{2.21}$$

Once the equilibrium solution q_α is known, the right-hand side of Eq (2.21) as well as the derivatives of ϕ in the right-hand side of Eq (2.20) can be computed. Note that the coefficient matrix in the equation above is the same stiffness matrix that was used in the equilibrium analysis – it is thus known in the decomposed form and it is a relatively cheap operation to get the solution against an additional right-hand side vector. Thus, solving Eq (2.21) and substituting the result into Eq (2.20) leads to the solution of the DSA problem.

The procedure presented above is called *direct differentiation method.* There is an alternative method called *adjoint system method* that can be used instead. It can be easily understood if Eq (2.21) is directly substituted into Eq (2.20)

$$\frac{d\phi}{dh} = \frac{d\phi}{dh}\Big|_{q_\alpha \neq q_\alpha(h)} + \frac{d\phi}{dq_\alpha}K^{-1}_{\alpha\beta}\frac{d(Q_\beta - F_\beta - F^c_\beta)}{dh}\Big|_{q_\alpha \neq q_\alpha(h)} \tag{2.22}$$

Introducing a vector λ_α and defining it as the solution of the following equation

$$K_{\alpha\beta}\lambda_\beta = \frac{d\phi}{dq_\alpha} \tag{2.23}$$

we can write

$$\frac{d\phi}{dh} = \frac{d\phi}{dh}\Big|_{q_\alpha \neq q_\alpha(h)} + \lambda_\beta\frac{d(Q_\beta - F_\beta - F^c_\beta)}{dh}\Big|_{q_\alpha \neq q_\alpha(h)} \tag{2.24}$$

In both methods, the arrays

$$\frac{d\phi}{dh}\Big|_{q_\alpha \neq q_\alpha(h)} \qquad \frac{d\phi}{dq_\alpha} \qquad \frac{dQ_\alpha}{dh}\Big|_{q_\alpha \neq q_\alpha(h)} \qquad \frac{d(F_\alpha + F^c_\alpha)}{dh}\Big|_{q_\alpha \neq q_\alpha(h)}$$

have to be computed and a system of equations with the coefficient matrix $K_{\alpha\beta}$ has to be solved against additional right-hand sides. The methods are fully equivalent numerically but their efficiency may be different, depending on the number of design parameters and responses (performances) in the problem.

While the differentiation of ϕ and Q_α is usually trivial, computation of the explicit design derivative of $F_\alpha + F_\alpha^c$ requires introduction of a fictitious design-independent reference configuration $\overline{C}$. This is because not only all the integrand components, but also the integration domain Ω, are design-dependent (Fig.1). This configuration is often associated with the parent configuration of an isoparametric finite element and so is it done in this paper (Fig.2).

Integration in Ω is thus replaced by integration in $\overline{\Omega}$. We have (cf Eq (2.10))

$$F_\alpha = \int_{\overline{\Omega}} B_{k\alpha}\sigma_k \bar{J}\, d\overline{\Omega} \tag{2.25}$$

and

$$\begin{aligned}
&\frac{dF_\alpha}{dh}\Big|_{q_\alpha \neq q_\alpha(h)} = \\
&= \int_{\overline{\Omega}} \Big(\frac{dB_{k\alpha}}{dh}\Big|_{q_\alpha \neq q_\alpha(h)} \sigma_k \bar{J} + B_{k\alpha}\frac{d\sigma_k}{dh}\Big|_{q_\alpha \neq q_\alpha(h)} \bar{J} + B_{k\alpha}\sigma_k \frac{d\bar{J}}{dh}\Big|_{q_\alpha \neq q_\alpha(h)} \Big)\, d\overline{\Omega} = \\
&= \int_{\Omega} \Big(\frac{dB_{k\alpha}}{dh}\Big|_{q_\alpha \neq q_\alpha(h)} \sigma_k + B_{k\alpha}\frac{d\sigma_k}{dh}\Big|_{q_\alpha \neq q_\alpha(h)} + B_{k\alpha}\sigma_k \frac{1}{\bar{J}}\frac{d\bar{J}}{dh}\Big|_{q_\alpha \neq q_\alpha(h)} \Big)\, d\Omega
\end{aligned} \tag{2.26}$$

with

$$\frac{d\sigma_k}{dh}\Big|_{q_\alpha \neq q_\alpha(h)} = \frac{dC_{kl}}{dh}\Big|_{q_\alpha \neq q_\alpha(h)} \varepsilon_l + C_{kl}\frac{d\varepsilon_l}{dh}\Big|_{q_\alpha \neq q_\alpha(h)} \tag{2.27}$$

$\bar{J}$ denotes here the gradient deformation from $\overline{\Omega}$ to Ω. Correct computation of design derivatives of strain and the geometric matrix $B_{k\alpha}$ requires that explicit dependence of each material point coordinates on h be taken into account.

The same issue refers to the contact contribution to the internal nodal force vector F^c. However, this time no transformations are necessary because F^c is defined as an integral in the configuration $\overline{C}^c$ (cf Eq (2.14)) which is design independent and can be identified with the configuration $\overline{C}$ for the contact zone. Explicit design differentiation of Eq (2.14) yields

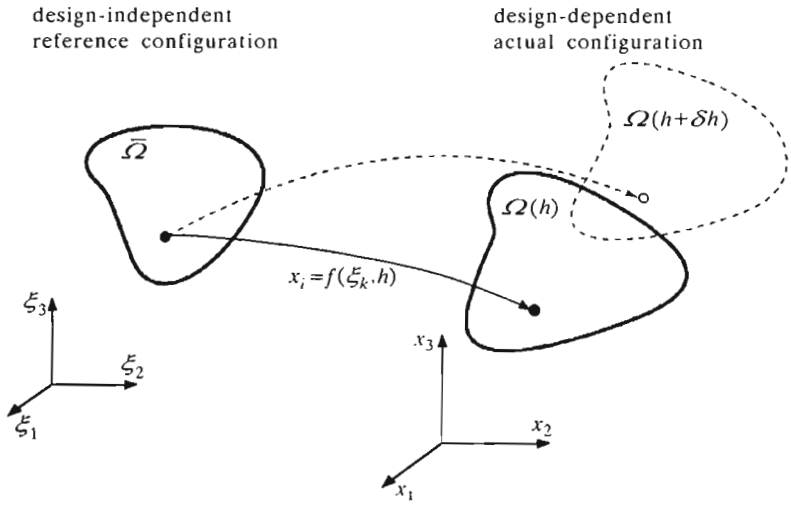

Fig. 1. Actual and design-independent reference configurations

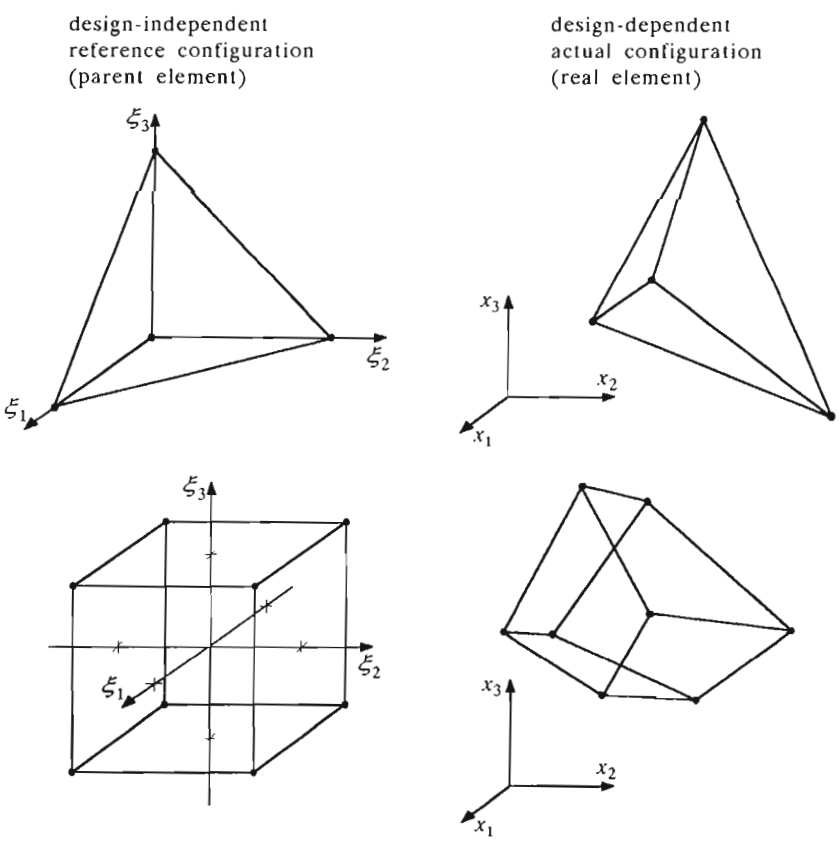

Fig. 2. Examples of isoparametric elements – actual and parent configurations

$$\left.\frac{dF_\alpha^c}{dh}\right|_{q_\alpha \neq q_\alpha(h)} = \tag{2.28}$$

$$= \int_{\bar{\Omega}^c} \Psi_{i\alpha;j}\Big(\left.\frac{dk'}{dh}\right|_{q_\alpha \neq q_\alpha(h)} F_{ji}^{-1} + k'(2\bar{F}_{lk}^{-1}\bar{F}_{ji}^{-1} - \bar{F}_{li}^{-1}\bar{F}_{jk}^{-1})\left.\frac{d\bar{F}_{kl}}{dh}\right|_{q_\alpha \neq q_\alpha(h)}\Big)\bar{J}^2\, d\Omega^c$$

2.4. Constitutive models

There are two types of the material considered in the analysed model of bone-implant system. These are: implant material and bone tissue.

Implant is assumed to be made of titanium alloy and it is modelled as elastic material with the Young modulus $E = 120$ GPa and the Poisson ratio $\nu = 0.3$.

Bone tissue is generally anisotropic viscoelastic material whose mechanical properties and anisotropy orientation depend on the bone type and position in the bone. They are also specific to the individual and may vary in time due to diseases and stress-induced remodelling. Here, we will neglect viscous effects appearing in the bone. We will also neglect material anisotropy. This is a significant simplification, especially for cortical bone, however, it can be justified at the stage of algorithm and software testing. Maximum values of anisotropic elastic moduli will be taken as valid in all material directions.

Spatial variation of the elastic constants in bone will be accounted for by distinguishing two material types: cortical bone (constituting an external layer of bone whose thickness is smaller at the bone head and larger in the shaft) and spongeous bone (filling the bone head and, partially, the shaft). Material properties of each tissue type will be taken as spatial average over each tissue volume and no spatial variations of material properties within each tissue type are considered.

Values of material constants assumed in the model are taken from experimental data published in the literature. Vast discrepancies between the results obtained by different authors can be observed, especially for spongeous bone (Martens et al., 1983; Cowin, 1989; Hobatho et al., 1997). In the analysis below we will take the following values:

- for cortical bone: $E = 17$ GPa, $\nu = 0.35$ (based on averaged data measured in orthotropic material tests reported by Cowin, 1989)
- for spongeous bone: $E = 0.5$ GPa (based on averaged data measured in orthotropic material tests by Hobatho et al., 1997, excluding data measured for the femoral head and neck), $\nu = 0.35$.

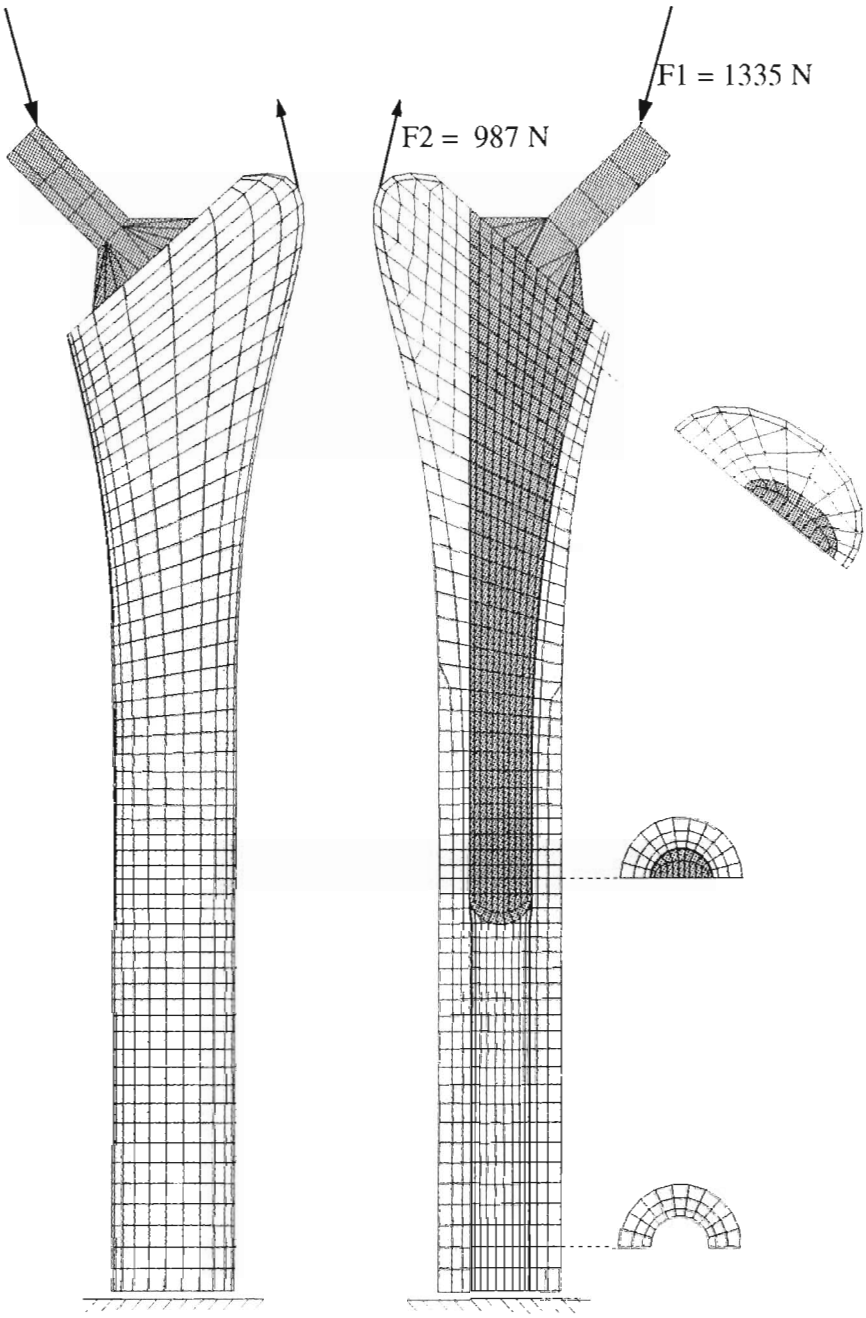

Fig. 3. Finite element model of the femur with a solid implant. Grey denotes implant, light-grey – cortical bone, white – spongeous bone, thick lines indicate sliding area

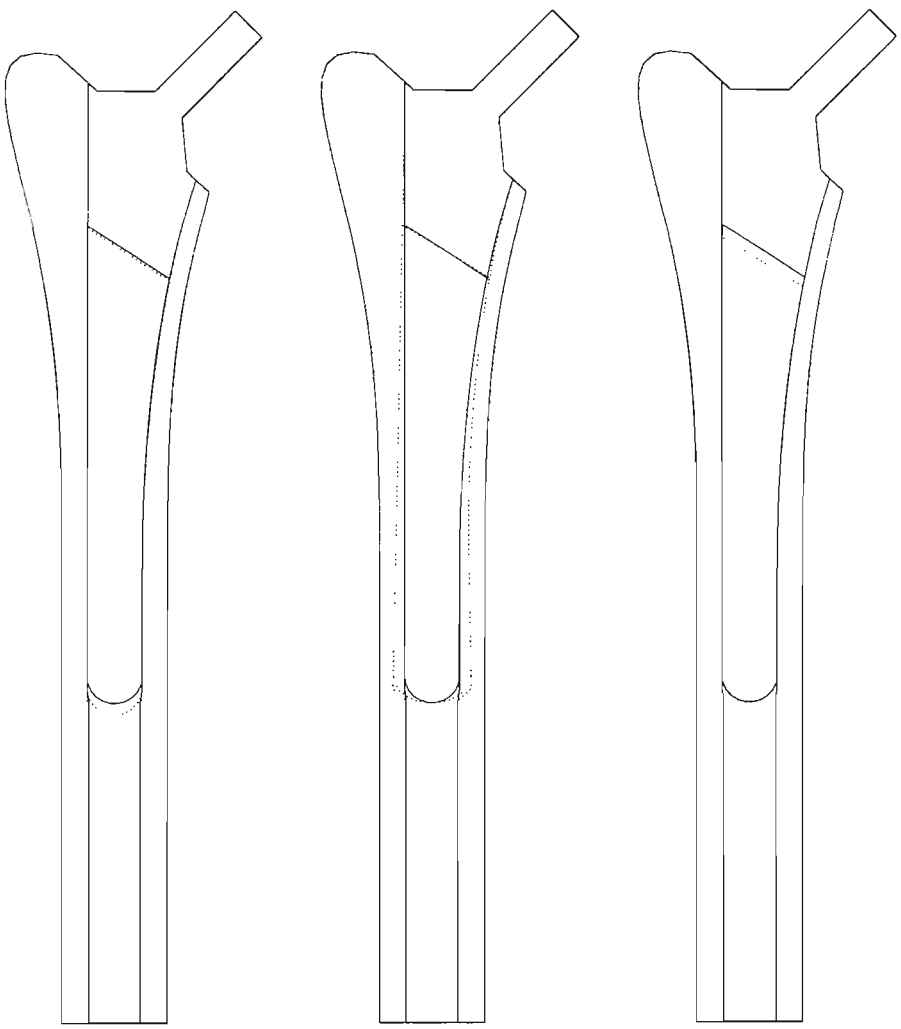

Fig. 4. Illustration to the design variables definition for a solid implant: dotted lines denote perturbed geometry for each variable

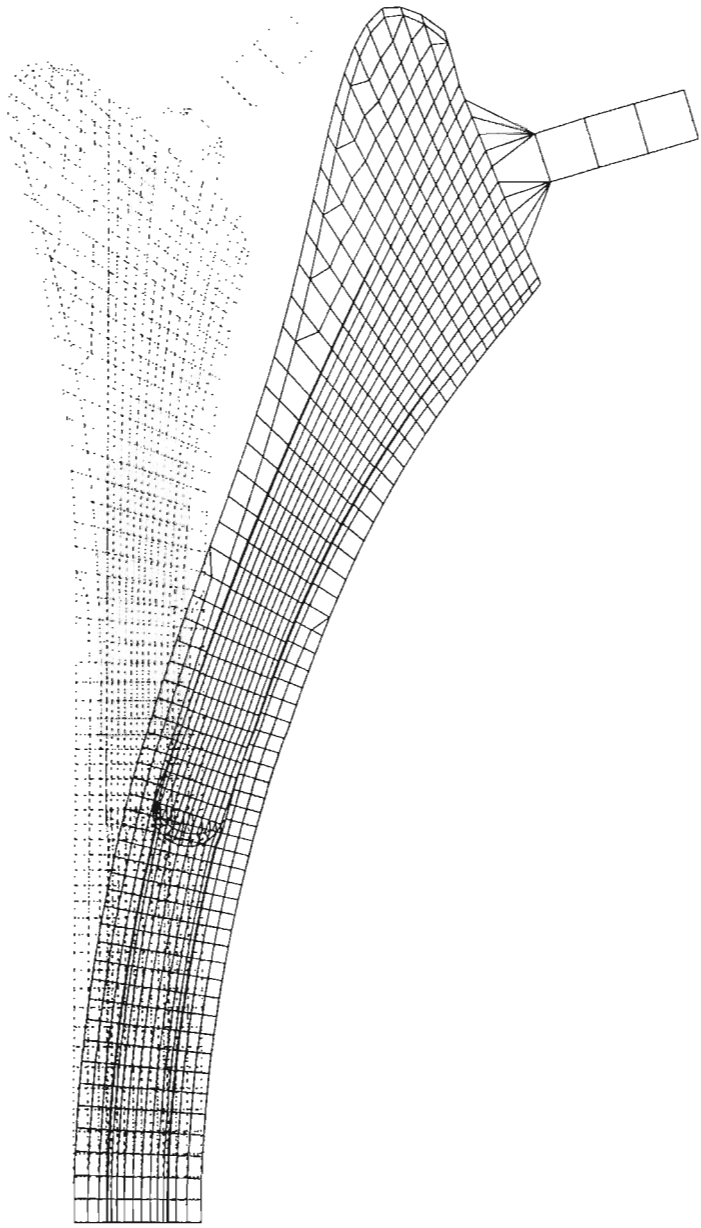

Fig. 5. Deformed mesh for a solid implant (displacement scaled by the factor 10)

3. Computational examples

Two cementless implant types were analysed: solid and hollow. The latter is not a typical one and is tested in order to determine how decreased implant stiffness affects stress concentrations in bone.

Geometry, finite element mesh with boundary conditions and loads for a bone with a solid implant are presented in Fig.3. Three-dimensional geometry is somewhat idealized by assuming semi-elliptic cross-section shapes at each level and planar symmetry with respect to the longitudinal plane intersecting medial and lateral bone contours. Symmetric half of the system is thus only analysed. Load values are assumed as for regular walking. Perfect bonding is assumed on the porous-coated implant surface part and frictionless contact condition on the remaining (smooth) part.

Both equilibrium and sensitivity analyses have been carriet out. The direct differentiation method has been employed in the DSA computations. Three design variables were considered: implant length, thickness of the distal implant end and height of the rough (porous-coated) implant surface zone (see Fig.4). Stress distributions in the bone tissue along the lateral and medial lines on the bone-implant surface (or free internal bone surface) are taken as design performances. The equivalent (Huber-Mises) stress is only considered.

Deformation of the loaded model is shown in Fig.5. The values of design performances and their sensitivities (derivatives with respect to each design variable) are shown in Fig.6 (medial side) and Fig.7 (lateral side).

As it can be seen from the results, the contact interaction between implant and bone arises, apart from the coated implant zone, at the distal (bottom) part of the implant on the lateral side and everywhere but the distal part of the implant on the medial side. This can be explained by the difference in deformation patterns of the relatively stiff stem and compliant bone shaft. Extreme stress concentrations occur predominantly on the lateral side, at the distal end (which is due to the bending reactions between the stem and shaft) and in the upper part (which is caused by the neighboring tendon which generates a loading force). On the medial side, increased stresses are only observed on the porous-coated implant part with an extreme value at the end of this zone. This value is slightly smaller (but comparable) than extreme values on the lateral side.

The sensitivity graphs indicate that implant length does not substantially affect stress distribution and its increase will affect a slight decrease of all the stress values around the concentration areas. Implant bottom end thickness considerably influence the stress concentration at the distal implant end (its

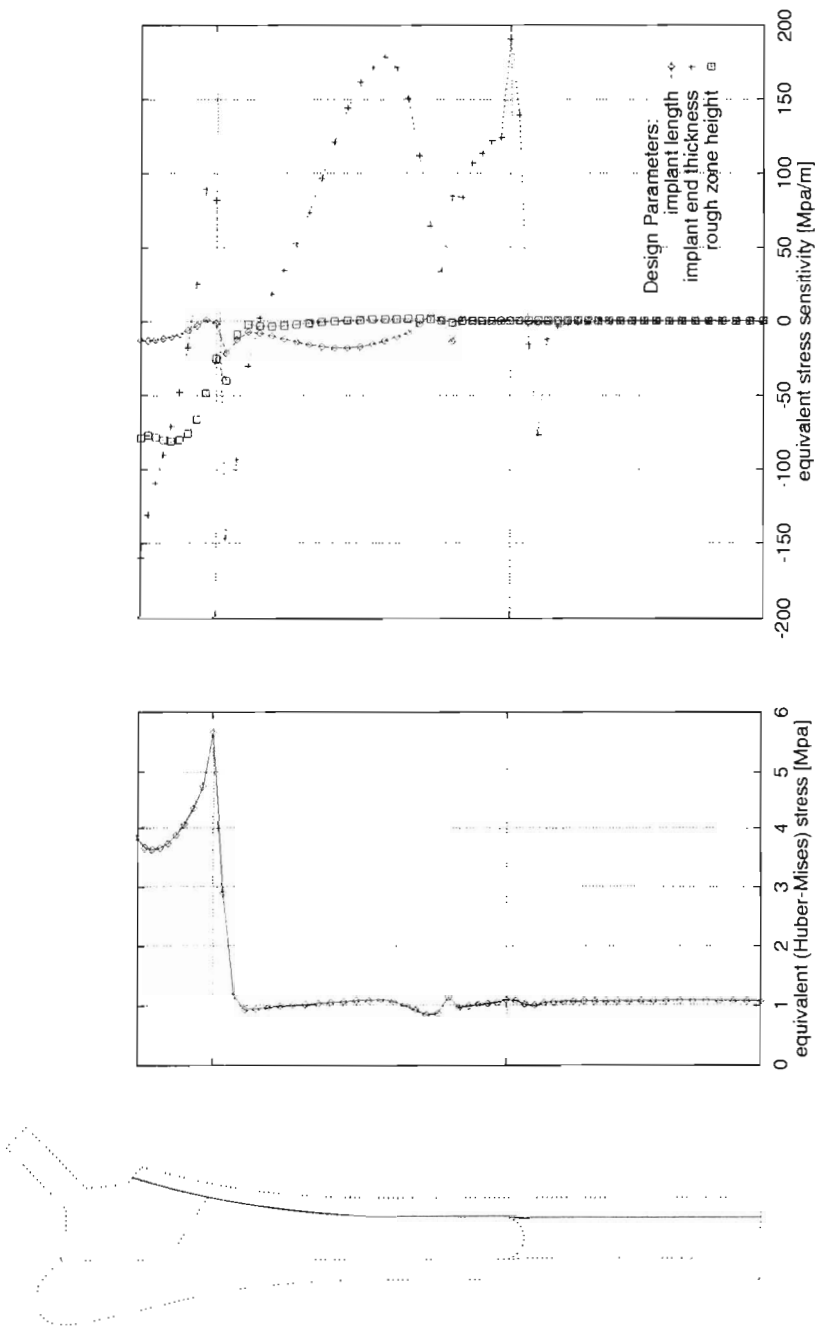

Fig. 6. Stress in bone tissue and its sensitivity on the medial bone-implant interface (thick line) for a solid implant

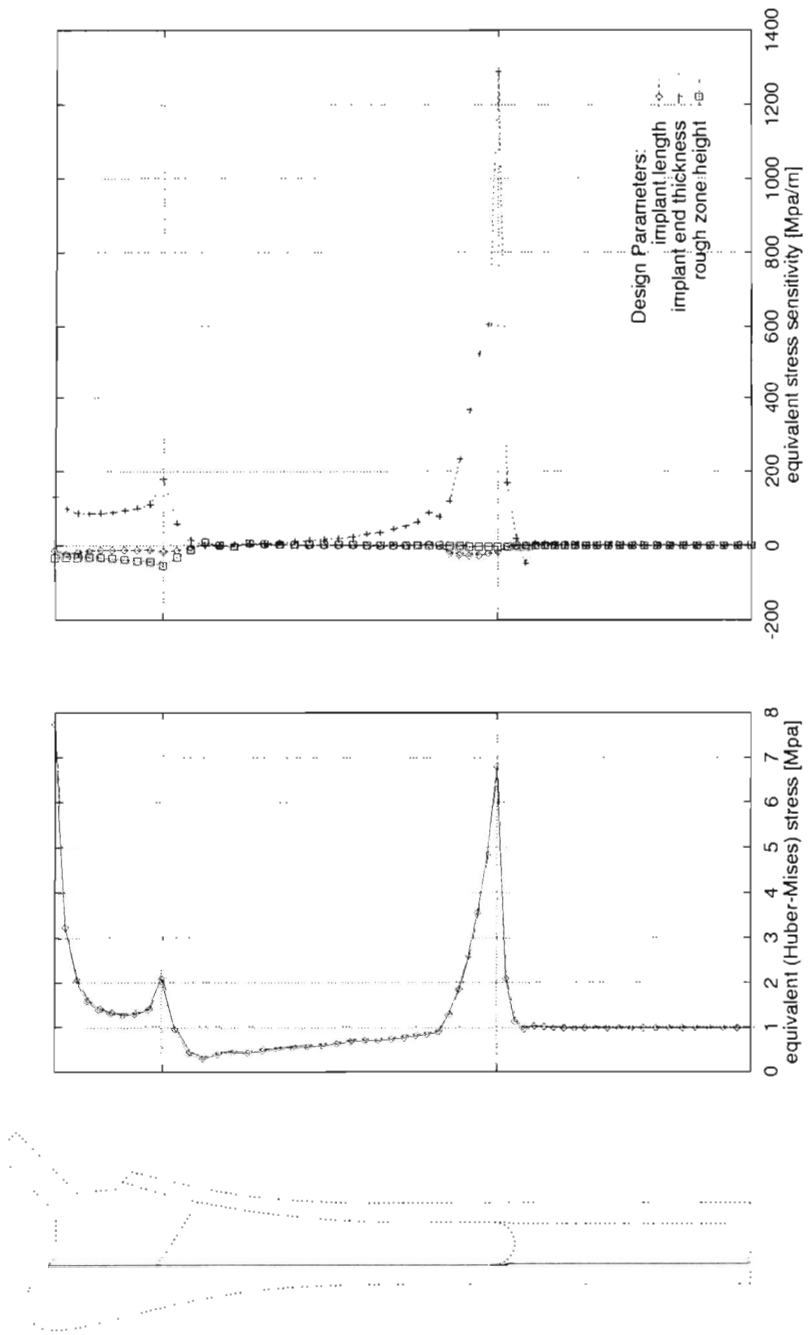

Fig. 7. Stress in bone tissue and its sensitivity on the lateral bone-implant interface (thick line) for a solid implant

increase will drop the stress values) and, to a much less extent, the remaining stress peaks, but its range of possible variations is much more limited than in the remaining design parameters. The coated zone height affects mainly the medial stress peak around the bottom end of the coated zone. Increase of the third parameter will cause a drop in high stress values on the coated interface. Also, a slight decrease of the peak stress is expected.

High stresses at the top end of lateral implant-bone interface appear to be essentially insensitive to the design parameters considered. Only the implant distal end thickness may affect it but to a relatively small extent. Modification of the interface geometry in this area (by decreasing the implant size in favor of more tissue left) may have a strong effect on the stress concentration but this would be very difficult from the technological point of view.

Another computational example is similar to the previous one but the solid implant is replaced by a hollow one. Since the large difference between stem and tissue stiffness is the main reason for uneven stress distributions in the implanted bone, the idea was to significantly decrease the stem stifness by removing a major part of its material. All remaining model characteristics remain the same. One additional design parameter has been introduced for this type of implant – the implant wall thickness.

The finite element mesh is presented in Fig.8. Fig.9 and Fig.10 present equilibrium and sensitivity results for this example. Stress concentrations are located in the same places as for the solid implant. Extreme stress values on the lateral side are considerably smaller, moreover, their sensitivities to the wall thickness are much higher than to the other parameters and indicate the rule *the thinner the wall the smaller the stress.* This is not the case, however, for the stresses on the upper medial side (at the coated zone end) where the stress concentration is even higher than for the solid implant and decreasing the wall thickness makes it even higher. Sensitivities of stresses to the other three parameters have similar distributions as for the solid implant.

4. Conclusions

An efficient numerical tool enabling the finite element analysis of bone-implant system supplemented with the design sensitivity analysis feature has been developed and successfully tested. The DSA computations are performed at low numerical cost and the code is suitable for applications to efficient 3D shape optimization algorithms.

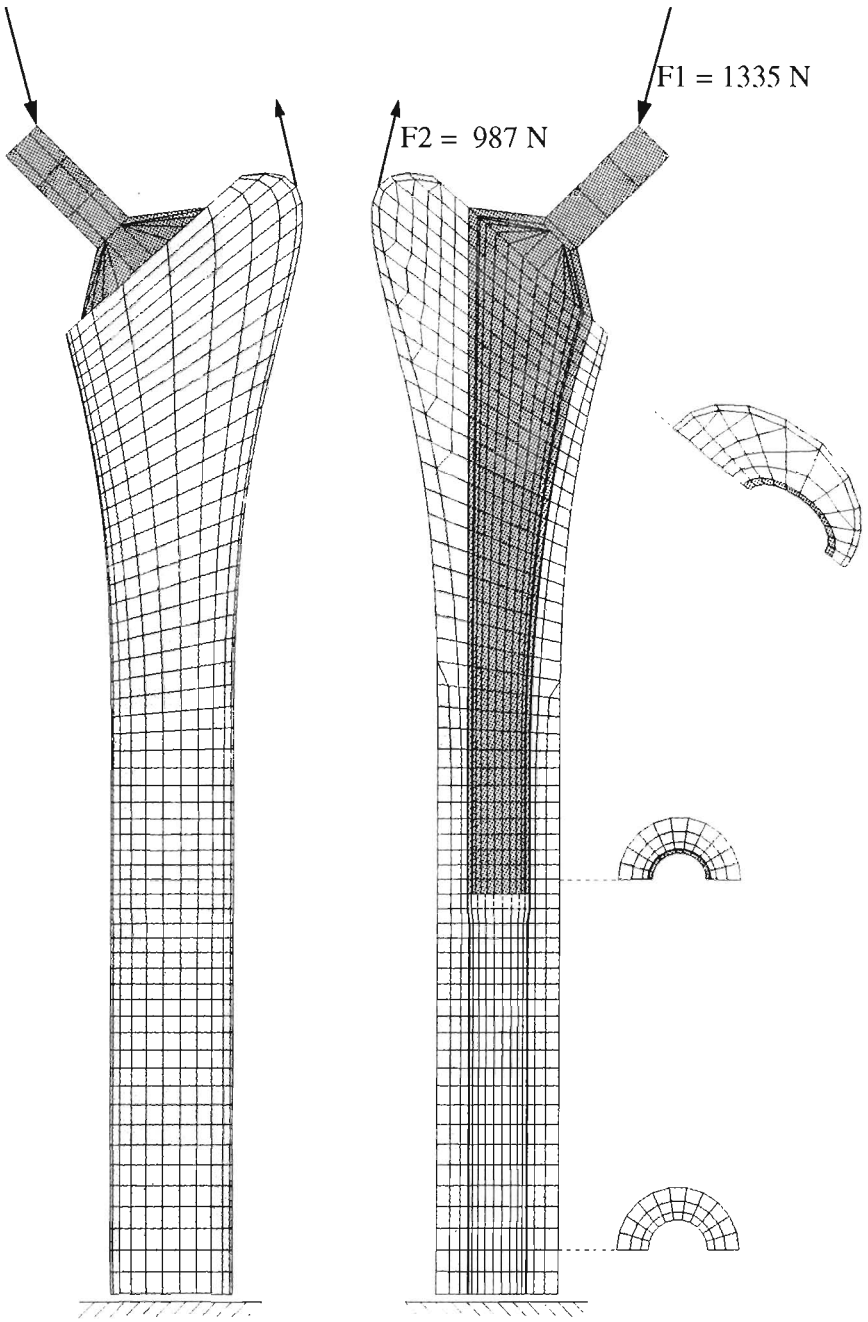

Fig. 8. Finite element model of the femur with a hollow implant (see explanations to Fig.3)

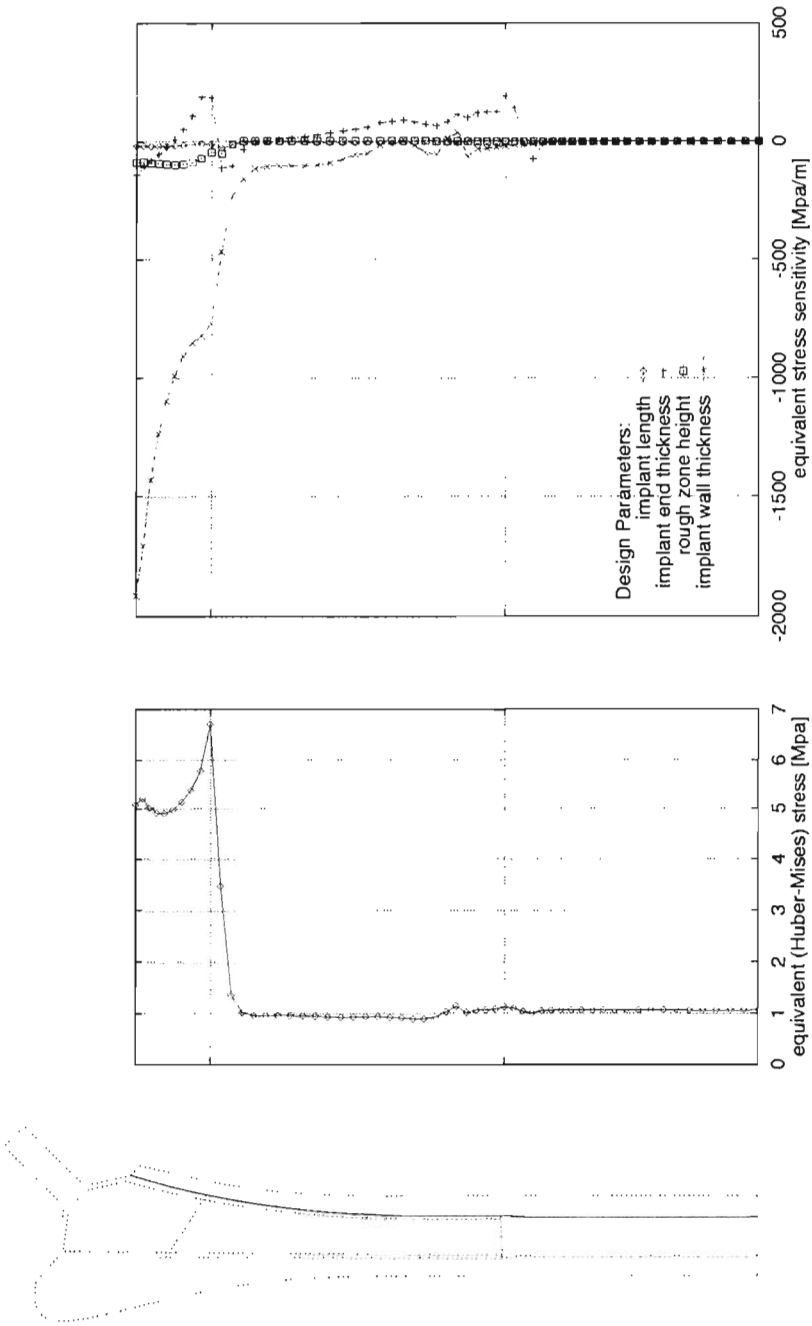

Fig. 9. Stress in bone tissue and its sensitivity on the medial bone-implant interface (thick line) for a hollow implant

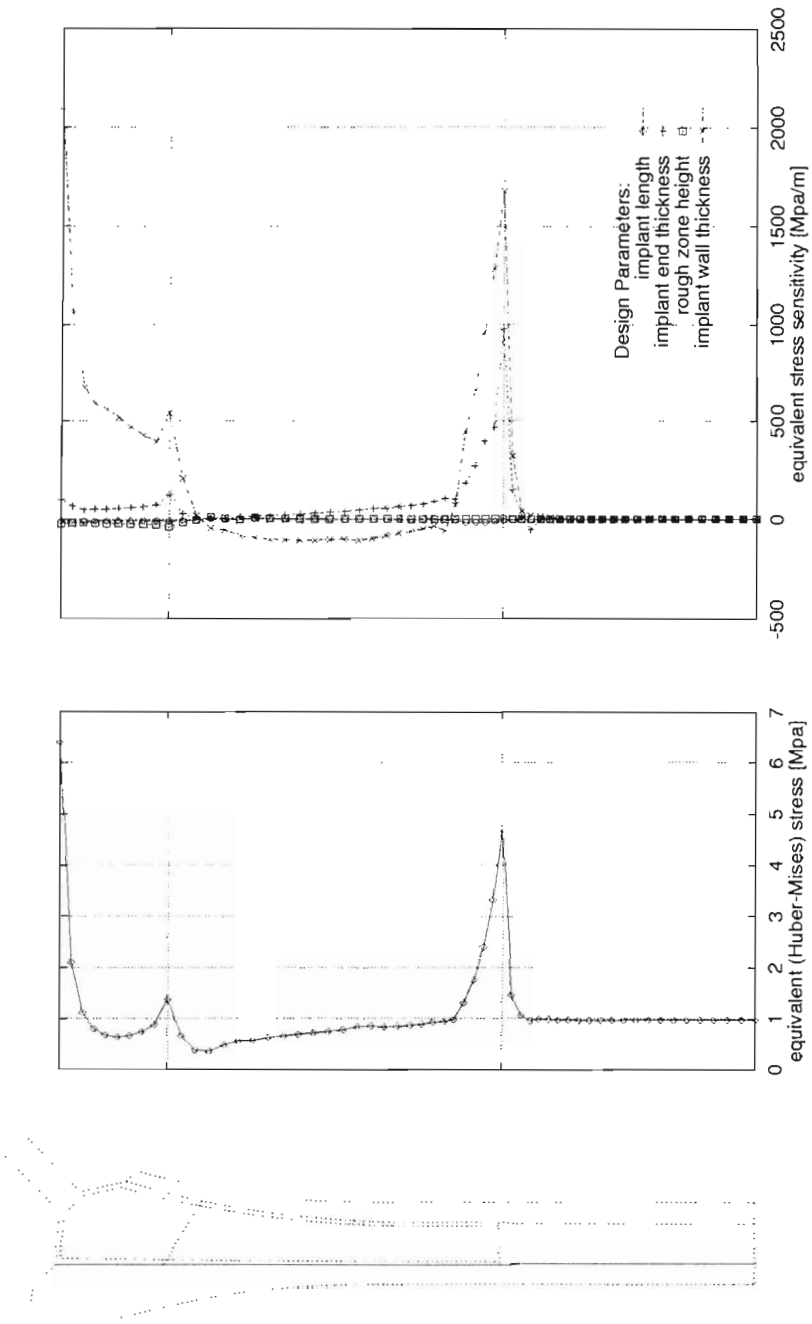

Fig. 10. Stress in bone tissue and its sensitivity on the lateral bone-implant interface (thick line) for a hollow implant

Bone-implant finite element models analysed in the numerical examples presented in the paper have idealized geometry, yet they provide a good qualitative information about the code abilities and, on the other hand, on the influence of geometric parameters of the implant stem on the stress distribution in the bone tissue. We can conclude that distal end thickness affects the peak values of stress concentration with the positive sign (i.e., the thinner implant distal end, the lower stress concentrations). The same can be said about the implant length and the coated zone height, but the values of sensitivities to these parameters are significantly smaller. Application of a hollow implant makes some stress concentration decrease while some others raise. This result needs further study including analysis of an implant with variable thickness, especially along its circumference.

Simplifications in bone geometric and material modelling may raise the question of reliability of the above results. The algorithm and the developed code can be, however, applied to more sophisticated finite element models with more details of geometry and distribution of material properties included.

Acknowledgement

Financial support from the State Committee for Scientific Research (KBN) under grant No. 8T11F 018 12 is gratefully acknowledged.

References

1. COWIN S., (edit.), 1989, *Bone mechanics*, CRC Press, Boca Raton
2. DAMMAK M., SHRIZI-ADL A., ZUKOR D.J., 1997, Analysis of Cementless Implants using Interface Nonlinear Friction – Experimental and Finite Element Studies, *Journal of Biomechanics*, **30**, 2, 121-129
3. MARTENS M., VAN AUDEKERCKE R., DELPORT P., DE MEESTER P., MULIER J.C., 1983, The Mechanical Characteristics of Cancellous Bone at the Upper Femoral Region, *Journal of Biomechanics*, **16**, 12, 971-983
4. HAUG E.J., CHOI K.K., KOMKOV V., 1986, *Design Sensitivity Analysis of Structural Systems*, Series in Math. Sci. Engrg., Academic Press
5. HEDIA H.S., BARTON D.C., FISHER J., IBRAHIM A., 1996, Shape Optimisation of a Charnley Prosthesis Based on the Fatigue Notch Factor, *Bio-Medical Materials and Engineering*, **6**, 199-217
6. HEDIA H.S., BARTON D.C., FISHER J., 1997, Material Optimisation of the Femoral Component of a Hip prosthesis Based on the Fatigue Notch Factor Approach, *Bio-Medical Materials and Engineering*, **7**, 83-98

7. HOBATHO M.-C., RHO J.Y., ASHMAN R.B., 1997, Anatomical Variation of Human Cancellous Bone Mechanical Properties in Vitro, In: G. Lowet et al. (eds.), *Bone Research in Biomechanis*, IOS Press

8. KANG Y.K, PARK H.C., YOUM Y., LEE I.K., AHN M.H., IHN J.C., 1993, Three Dimensional Shape Reconstruction and Finite Element Analysis of Femur Before and After the Cementless Type of Total Hip Replacement, *Journal of Biomedical Engineering*, **15**, 497-504

9. KLEIBER M., ANTÚNEZ H., HIEN T.D., KOWALCZYK P., 1997, *Parameter Sensitivity in Nonlinear Mechanics*, Wiley, Chichester

10. KUIPER J.H., HUISKES R., 1997, Mathematical Optimization of Elastic Properties: Application to Cementless Hip Stem Design, *Transactions of the ASME, Journal of Biomechanical Engineering*, **119**, 166-174

11. KEAVENY T.M., BARTEL D.L., 1993, Effect of Porous Coating and Collar Support on Early Load Transfer for a Cementless Hip Prosthesis. *Journal of Biomechanics*, **26**, 10, 1205-1216

12. KOWALCZYK P., 1994, Finite-Deformation Interface Formulation for Frictionless Contact Problems, *Communications in Numerical Methods in Engineering*, **10**, 879-893

13. MANN K.A., BARTEL D.L., WRIGHT T.M., BURSTEIN A.H., 1995, Coulomb Frictional Inerfaces in Modeling Cemented Total Hip Replacements: a More Realistic Model, *Journal of Biomechanics*, **28**, 9, 1067-1078

14. MCNAMARA B.P., CRISTOFOLINI L., TONI A., TAYLOR D., 1997, Relationship between Bone-Prosthesis Bonding and Load Transfer in Total Hip Reconstruction, *Journal of Biomechanics*, 30, 6, 621-630

15. YANG R.J., CHOI K.K., CROWNINSHIELD R.D., BRAND R.A., 1984, Design Sensitivity Analysis: A New Method for Implant Design and a Comparison with Parametric Finite Element Analysis, *Journal of Biomechanics*, **17**, 11, 849-854

16. ZIENKIEWICZ O.C., 1977, *The Finite Element Method*, McGraw-Hill

Numeryczne wyznaczanie wrażliwości rozkładu naprężeń w kości na parametry geometryczne endoprotezy

Streszczenie

Jednym z poważnych mankamentów endoprotetyki stawów jest odrywanie się implantu od cementu lub kości. Główną przyczyną tego zjawiska są koncentracje naprężeń na powierzchni implantu. Optymalizacja kształtu implantu jest uważana za

naturalną drogę do przeciwdziałania temu zjawisku. Ważnym narzędziem w algorytmach optymalizacji jest analiza wrażliwości parametrycznej (DSA).

Praca przedstawia sformułowanie zagadnienia wrażliwości w zdyskretyzowanym ujęciu metody elementów skończonych. Analizowana jest kość udowa z implantem bezcementowym o powierzchni gładkiej, a w górnej części porowatej. Przykłady numeryczne przedstawiają koncentracje naprężeń w tkance kostnej i ich wrażliwość na różne parametry kształtu implantu.

Manuscript received January 5, 1999; accepted for print January 25, 1999